Periplasmic depolymerase provides insight into ABC transporter-dependent secretion of bacterial capsular polysaccharides

Sean D. Liston[a], Stephen A. McMahon[b], Audrey Le Bas[c], Michael D. L. Suits[d], James H. Naismith[c,1], and Chris Whitfield[a,1]

[a]Department of Molecular and Cellular Biology, University of Guelph, Guelph, ON N1G 2W1, Canada; [b]Biomedical Sciences Research Complex, The University of St. Andrews, St. Andrews KY16 9ST, United Kingdom; [c]Division of Structural Biology, Nuffield Department of Medicine, University of Oxford, Oxford OX3 7BN, United Kingdom; and [d]Department of Chemistry and Biochemistry, Wilfrid Laurier University, Waterloo, ON N2L 3C5, Canada

Edited by Joe Lutkenhaus, University of Kansas Medical Center, Kansas City, KS, and approved April 13, 2018 (received for review January 23, 2018)

Capsules are surface layers of hydrated capsular polysaccharides (CPSs) produced by many bacteria. The human pathogen *Salmonella enterica* serovar Typhi produces "Vi antigen" CPS, which contributes to virulence. In a conserved strategy used by bacteria with diverse CPS structures, translocation of Vi antigen to the cell surface is driven by an ATP-binding cassette (ABC) transporter. These transporters are engaged in heterooligomeric complexes proposed to form an enclosed translocation conduit to the cell surface, allowing the transporter to power the entire process. We identified Vi antigen biosynthesis genetic loci in genera of the *Burkholderiales*, which are paradoxically distinguished from *S.* Typhi by encoding VexL, a predicted pectate lyase homolog. Biochemical analyses demonstrated that VexL is an unusual metal-independent endolyase with an acidic pH optimum that is specific for O-acetylated Vi antigen. A 1.22-Å crystal structure of the VexL-Vi antigen complex revealed features which distinguish common secreted catabolic pectate lyases from periplasmic VexL, which participates in cell-surface assembly. VexL possesses a right-handed parallel β-superhelix, of which one face forms an electropositive glycan-binding groove with an extensive hydrogen bonding network that includes Vi antigen acetyl groups and confers substrate specificity. VexL provided a probe to interrogate conserved features of the ABC transporter-dependent export model. When introduced into *S.* Typhi, VexL localized to the periplasm and degraded Vi antigen. In contrast, a cytosolic derivative had no effect unless export was disrupted. These data provide evidence that CPS assembled in ABC transporter-dependent systems is actually exposed to the periplasm during envelope translocation.

bacterial cell surface | capsular polysaccharide | *Salmonella enterica* | glycosidase | glycan export

Most bacterial cell surfaces are dominated by carbohydrate-containing molecules, which modulate interactions with the external environment. Some bacteria, including several significant human pathogens, produce a capsule, which is a cell-surface layer composed of hydrated polysaccharide. The mechanism for tethering the polysaccharide to the cell surface is not known in all cases, but prevalent systems in Gram-negative bacteria use terminal glycolipids (1, 2). Capsular polysaccharides (CPSs) allow some commensals to influence homeostasis of the host immune system, mediate host interactions by plant symbionts, are receptors for bacteriophages, and are established virulence factors in pathogens. In pathogens, capsules interrupt innate immune responses by masking cell-surface pathogen-associated molecular patterns (PAMPs), reducing serum complement deposition and limiting phagocytosis (3, 4).

Selective pressures have led to enormous diversity in CPS structures, reflected as variation in monosaccharide composition, linkage, and nonsugar decoration. More than 80 CPS structures have been identified in *Escherichia coli* isolates alone (5). Despite structural diversity in CPS glycans, the protein machinery for their assembly and secretion is conserved. The two CPS assembly strategies in Gram-negative bacteria employ different modes of translocation across the inner membrane (5). This step is facilitated by either a multidrug/oligosaccharidyl-lipid/polysaccharide export (MOP) "flippase" (Wzx) (reviewed in ref. 6), or an ATP-binding cassette (ABC) transporter (reviewed in refs. 2 and 7). This work focuses on the latter strategy, which is often referred to by its classification in *E. coli* as "group 2" capsule assembly (5). This strategy is shared by a range of encapsulated pathogens including meningococci, *Haemophilus influenzae*, *Campylobacter jejuni*, *Bordetella pertussis*, and *Salmonella enterica* serovar Typhi (2). Prototypes for group 2 ABC transporter-dependent CPS assembly are provided by *E. coli* serotype K1 and K5 CPSs. These CPS glycans are assembled at the cytoplasm-membrane interface on a conserved glycolipid consisting of ∼5 to 9 β-linked 3-deoxy-β-D-*manno*-oct-2-ulosonic acid (Kdo) residues attached to a reducing terminal (lyso) phosphatidylglycerol (*lyso*PG) (1). The resulting glycolipid is the acceptor for different CPS structures in a wide range of bacterial species (2, 7). Serotype-specific glycosyltransferases extend *lyso*PG-oligo-Kdo in the cytoplasm (1, 7). The glycolipid terminus is

Significance

Capsules are critical virulence determinants for bacterial pathogens. They are composed of capsular polysaccharides (CPSs) with diverse structures, whose assembly on the cell surface is often powered by a conserved ABC transporter. Current capsule-assembly models include a contiguous trans-envelope channel directing nascent CPSs from the transporter to the cell surface. This conserved apparatus is an attractive target for antivirulence antimicrobial development. This work describes a CPS depolymerizing lyase enzyme found in the *Burkholderiales* and unique structural features that define its mechanism, CPS specificity, and evolution to function in the periplasm in a noncatabolic role. The activity of this enzyme provides evidence that CPS assembled in an ABC transporter-dependent system is exposed to periplasm during translocation to the cell surface.

Author contributions: S.D.L., S.A.M., J.H.N., and C.W. designed the study; S.D.L., S.A.M., and A.L.B. performed experiments; S.D.L., S.A.M., M.D.L.S., J.H.N., and C.W. analyzed the data; and S.D.L., S.A.M., J.H.N., and C.W. wrote the paper.

The authors declare no conflict of interest.

This article is a PNAS Direct Submission.

Data deposition: The atomic coordinates and structure factors have been deposited in the Protein Data Bank, www.wwpdb.org (PDB ID code 6FI2).

[1]To whom correspondence may be addressed. Email: naismith@strubi.ox.ac.uk or cwhitfie@uoguelph.ca.

This article contains supporting information online at www.pnas.org/lookup/suppl/doi:10.1073/pnas.1801336115/-/DCSupplemental.

Published online May 7, 2018.

likely recognized by the ABC transporter as an export signal (reviewed in ref. 2).

Glyco-ABC transporters are composed of two copies each of a transmembrane domain (TMD) and a nucleotide-binding domain (NBD), encoded by *kpsM* and *kpsT* in *E. coli*, respectively. ATP binding and hydrolysis in the NBD dimer drives conformational changes in the TMD dimer that power CPS secretion across the inner membrane (reviewed in refs. 2 and 8). Translocation of CPS across the periplasm and outer membrane employs a heterooligomeric complex composed of polysaccharide copolymerase (PCP) and outer membrane polysaccharide export (OPX) proteins (reviewed in ref. 9). The current model proposes that these components form a contiguous envelope-spanning channel resembling some bacterial tripartite drug efflux pumps. In efflux pumps, an inner membrane flippase (10), or ABC transporter (11), interfaces with the outer membrane porin (TolC) through interactions with a periplasmic adaptor protein complex. Available structure and protein interaction data (reviewed in ref. 5) drive the hypothesis that the CPS ABC transporter resides within a complex composed of the transporter, a PCP protein adaptor, and an OPX channel (Fig. 1). However, there is currently no atomic-level data for PCP or OPX proteins from ABC transporter-dependent systems, and this hypothetical export pathway has not been interrogated experimentally.

Vi antigen is a CPS produced by *S. enterica* serovar Typhi, the etiological agent of typhoid fever, a disease that afflicts millions each year. Vi antigen is composed of the repeating monosaccharide unit $[\rightarrow 4)$-α-D-Gal*N*AcA-$(1\rightarrow]_n$ which is nonstoichiometrically O-acetylated at C-3 (12). It is exploited in current vaccines (13). Like K1 and K5 CPSs, Vi antigen assembly employs an ABC transporter complex, which is encoded by *vexB* (TMD), *vexC* (NBD), *vexD* (PCP), and *vexA* (OPX) (Fig. 1) (14, 15). However, the Vi antigen glycolipid terminus and synthesis machinery is distinct from *E. coli* prototypes in that Vi antigen possesses a reducing-terminal *N*-acetylhexosamine residue decorated with two β-hydroxyacyl chains, instead of oligo-Kdo-*lyso*PG (16).

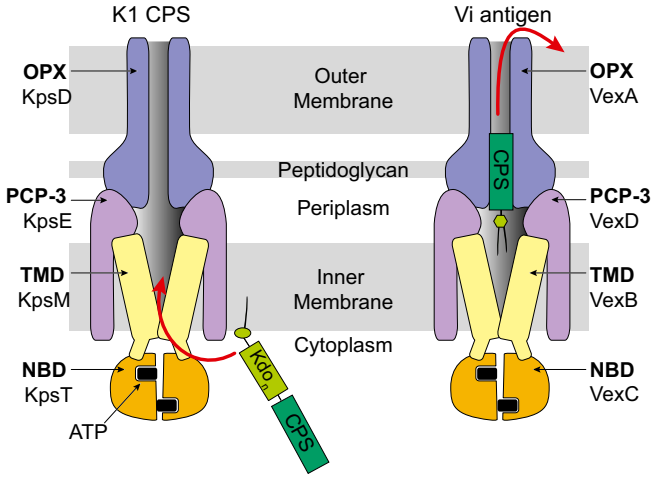

Fig. 1. Model for ABC transporter-dependent CPS assembly in Gram-negative bacteria. The figure illustrates systems from an *E. coli* group 2 prototype and *S.* Typhi Vi antigen at different conceptual states in the CPS envelope translocation process. CPS glycans are assembled from NDP-activated glycose residues by cytosolic glycosyltransferase enzymes at the cytoplasm-membrane interface (*SI Appendix*, Fig. S1*B*), before recognition and export by the ABC transporter. The nascent glycans possess different terminal glycolipids. Binding and hydrolysis of ATP by the cytoplasmic NBD protein dimer drives conformational changes in the TMD that power secretion of CPS across the inner membrane. The transporter is proposed to engage the outer membrane OPX channel via interaction with a PCP adaptor.

Genes for Vi antigen production are found in some soil bacteria, including *Achromobacter denitrificans* and *Bordetella petrii* (16). Paradoxically, these Vi antigen-assembly systems include VexL, a predicted homolog of pectate lyases that depolymerizes Vi antigen in vitro; VexL is absent from *S.* Typhi (16). To determine whether VexL was simply a catabolic enzyme with broad specificity, we investigated its structure and function. We found that VexL is a periplasmic Vi antigen-specific lyase enzyme. The structure of the VexL–Vi antigen complex was solved by X-ray crystallography and defined amino acid residues important for activity and specificity. Depolymerizing enzymes are unprecedented in CPS assembly systems and conflict with current conceptual models for secretion that include a privileged periplasmic channel. The discovery of VexL provided an opportunity to test this model. We therefore examined the effect of introducing VexL into *S.* Typhi, which revealed insights into the molecular mechanism of the ABC transporter-dependent CPS secretion that is conserved in many clinically important bacterial pathogens.

Results

VexL Is a Pectate Lyase Homolog Conserved in *Burkholderiales* Vi Antigen Assembly Systems. We identified *vexL* in the Vi antigen biosynthesis genetic locus (*viaB*) of *Achromobacter denitrificans* (16). Homologs of VexL belonged to the ambrosia allergen protein family, which contains pectate lyase enzymes (Conserved Domain Database) (16, 17). The structure of Vi antigen superficially resembles pectin (which has the repeat unit structure $[\rightarrow 4)$-D-GalA-α-$(1\rightarrow]_n$), and we hypothesized that VexL was a pectate lyase homolog with Vi antigen depolymerase activity (16). Vi-antigen depolymerization had been demonstrated in vitro (16), but substrate specificity remained untested. Furthermore, the presence of a signal sequence (mean D score residues 1 to 23 = 0.73, cutoff = 0.57, SignalP4.1) (18) suggested that VexL is an exported protein but gave no insight into its final cellular location or biological function.

To expand our understanding of this enzyme, position-specific iterative BLAST (19) was used to identify additional homologs of VexL; hits were plant pectate lyases or bacterial enzymes within the Order *Burkholderiales* (Fig. 2). The *Burkholderiales* homologs shared 65 to 89% identity with *A. denitrificans* VexL. Interestingly, classical characterized bacterial pectate lyases A and C from *Dickeya dadanti* (20, 21) and *Bacillus subtilis* (22) were not identified, for example. When the phylogeny of these enzymes was investigated, bacterial VexL homologs and known bacterial pectate lyases clustered separately from representatives from plants (Fig. 2). Furthermore, *Burkholderiales* VexL form a distinct clade separate from characterized bacterial pectate lyases. The genes encoding VexL-clade enzymes were all located adjacent to genes encoding homologs of Vi antigen biosynthesis and export proteins (*SI Appendix*, Fig. S1*A*), supporting the hypothesis that VexL is specifically involved in Vi antigen assembly and/or processing rather than a catabolic pectinase.

VexL Is a Vi Antigen-Specific Lyase. We previously used VexL to reduce the molecular weight of Vi antigen to isolate the terminal glycolipid residue (16). The apparent molecular weight of Vi antigen decreased in PAGE when incubated with VexL, and purified glycolipids possessed a nonreducing terminal anhydro residue (16) characteristic of lyase enzyme digestion (23, 24). To investigate this activity in more detail, VexL was incubated with purified Vi antigen, and reaction products were analyzed by HPLC coupled to mass spectrometry (MS). Mass spectra revealed species that differed by 217.059 *m*/*z*, which correspond to oligosaccharides of Gal*N*AcA, two to seven residues in length (Fig. 3 and *SI Appendix*, Table S1). No monosaccharides were detected, indicative of an endo-acting enzyme. MS also revealed species that differed by −42.011 and −18.011 *m*/*z*, which represent nonstoichiometric O-acetylation of the polysaccharide,

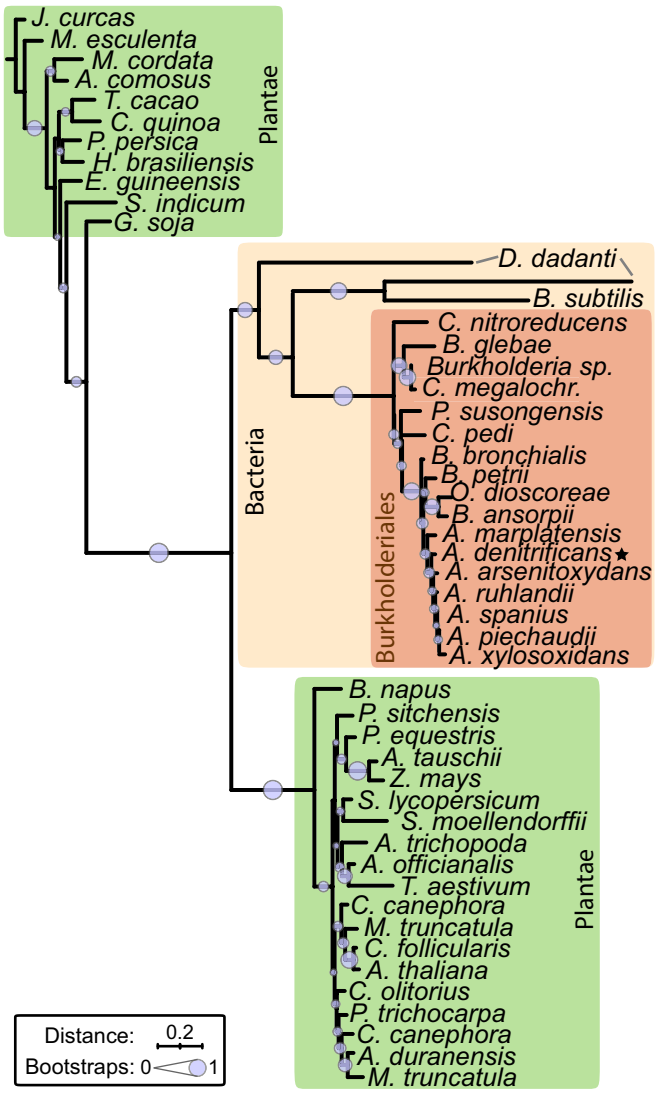

Fig. 2. Phylogeny of VexL pectate lyases. The figure depicts a phylogram of VexL homologs, identified by position-specific iterative BLAST (19) of VexL from *Achromobacter denitrificans*. The maximum-likelihood phylogram was generated from 100 bootstrapped datasets using PhyML3.0 (64) and visualized using iTOL (65). GenBank (84) accession numbers for VexL homologs are listed in *SI Appendix, Materials and Methods*. Bootstraps are labeled as purple circles.

and water loss, respectively. In all of the products, VexL creates a nonreducing 4-deoxy-2-*N*-acetyl-α-D-*galact*-4-enuronosyl residue. This modification appears in MS as an "anhydro" residue at the nonreducing terminus (Fig. 3 and *SI Appendix*, Table S1). No hydrated species (i.e., hydrolase products) were detected. Cross-ring fragmentation products in MS^2 were consistent with this terminal modification (*SI Appendix*, Fig. S2). Formation of 4-deoxy-α-D-*galact*-4-enuronosyl residues, which absorb at 232 nm (*SI Appendix*, Fig. S3*A*), confirmed a lyase mechanism rather than hydrolase and offered the opportunity to follow the reaction by spectrophotometry (25). VexL degraded Vi antigen, generating 3.2 $\mu mol \cdot min^{-1} \cdot mg^{-1}$ nonreducing termini at its pH optimum of 5.5 (*SI Appendix*, Fig. S3*B*). Product formation was dependent on O-acetylation of the glycan; no activity was detected for de-O-acetylated Vi antigen or pectate (*SI Appendix*, Fig. S3*A*). VexL activity was unaffected by EDTA, indicating no divalent cation(s) was required for catalysis (*SI Appendix*, Fig. S3*A*).

Structure of VexL. To further characterize VexL, its 3D structure was determined by X-ray crystallography. The gene construct encoded the entire *A. denitrificans* VexL preprotein, including the predicted N-terminal signal sequence and a C-terminal affinity tag. VexL-His_6 was expressed in *E. coli* and purified from the periplasm to ensure proper folding of the mature protein, that might be affected by the oxidizing periplasmic environment and signal peptidase processing. Initial optimized VexL crystals diffracted to ≥2.8 Å (space group $P\ 3_1$). To improve resolution, we incubated VexL-His_6 with purified Vi antigen and screened for new crystallization conditions. The addition of the glycan did not affect the melting temperature of VexL; the T_m was 59.5 °C with 5 mg/mL Vi antigen. The resulting tetragonal crystals diffracted to 1.22 Å (space group $P\ 4_2\ 2_1\ 2$). These data were phased by molecular replacement, and discussion focuses on this structure (Table 1). The asymmetric unit contains one copy of VexL, a malonate ion (buffer), and a trisaccharide of Vi antigen ([→4)-D-Gal*N*AcA3Ac-α-(1→]$_3$). In contrast, the apo-structure was largely incomplete and differed from the glycan-bound structure by 0.45 Å rmsd. Amino acid residues of VexL are hereafter numbered based on the full-length preprotein sequence. VexL currently represents the most complete and highest resolution structure for any active pectate lyase in the PDB.

The VexL structure contains density for residues Cys^{28}-Pro^{392}, Arg^{395}-Gly^{402}, and two His residues from the affinity tag. There are three disulfide linkages: Cys^{28}-Cys^{35}, Cys^{279}-Cys^{296}, and Cys^{364}-Cys^{400}. The majority of VexL is composed of a right-handed parallel β-helix with three "faces" composed of parallel β-sheets (Fig. 4 *A* and *B*). Each β-strand is connected to the adjacent one by a short two- to four-residue loop. This forms a compact "core," which is packed with ordered arrays of aliphatic and hydrophobic amino acids, contributed by each "rung" in the β-helix (labeled 1 to 10) (Fig. 4*B*). The regular pattern is interrupted by insertions that comprise a loop with an α-helix (rung 6; Leu^{199}-Arg^{218}), a long loop with an α-helix (rung 9; Asn^{273}-Arg^{305}) that is stabilized by a disulfide linkage (Cys^{279}-Cys^{296}) and salt bridge (Asp^{252}-Arg^{277}), and a loop with an α-helix (rung 9; Asn^{314}-Asp^{330}) (*SI Appendix*, Fig. S4*A*). These insertions result in two faces of the β-helix being buried and the third face forming the base of an extensive groove. This groove is populated by conserved (Fig. 4*C*) and positively charged amino acids (Fig. 4*D*). The N terminus (Cys^{28}-Pro^{85}) comprises two α-helices, a β-strand, and a long loop. The long loop and long α-helix pack against one face of the β-helix. The shorter α-helix and β-strand pack against the top end of the β-helix. The C terminus (Gly^{343}-Gly^{402}) forms loops and a short α-helix that cap the bottom end of the β-helix and then pack against the same β-sheet as the N terminus and its neighbor (Fig. 5).

The cocomplex reveals clear electron density for three sugar residues of Vi antigen, positioned within the large groove highlighted above (Fig. 4*E*). There is additional density that suggests a longer polymer, but we were unable to unambiguously model beyond the trisaccharide. The long axis of the trisaccharide molecule and the VexL β-helix align; the reducing sugar sits at the C-terminal end of the β-helix, essentially level with the "base" of the structure. The carboxylate group of the nonreducing sugar makes a bidentate salt contact with the side chain of Arg^{235} while the oxygen of the *N*-acetyl group is hydrogen bonded to Lys^{195} (*SI Appendix*, Fig. S5*G*). The O4 of this sugar makes a hydrogen bond with Arg^{232}, and the pyranose ring oxygen (O5) hydrogen bonds to Arg^{232} and water. There was no additional difference density for an *O*-acetyl group of this sugar. The importance of these amino acids was probed by site-directed mutagenesis. Purified periplasmic VexL K195A, R232K, R232A, and R235A (*SI Appendix*, Fig. S3*C*) were inactive in in vitro assays monitoring depolymerization or formation of unsaturated termini (*SI Appendix*, Fig. S3 *E* and *F*), despite remaining folded (*SI Appendix*, Fig. S3*D*). VexL R235K had 5% of WT activity. Gln^{237} hydrogen bonds to Arg^{235}

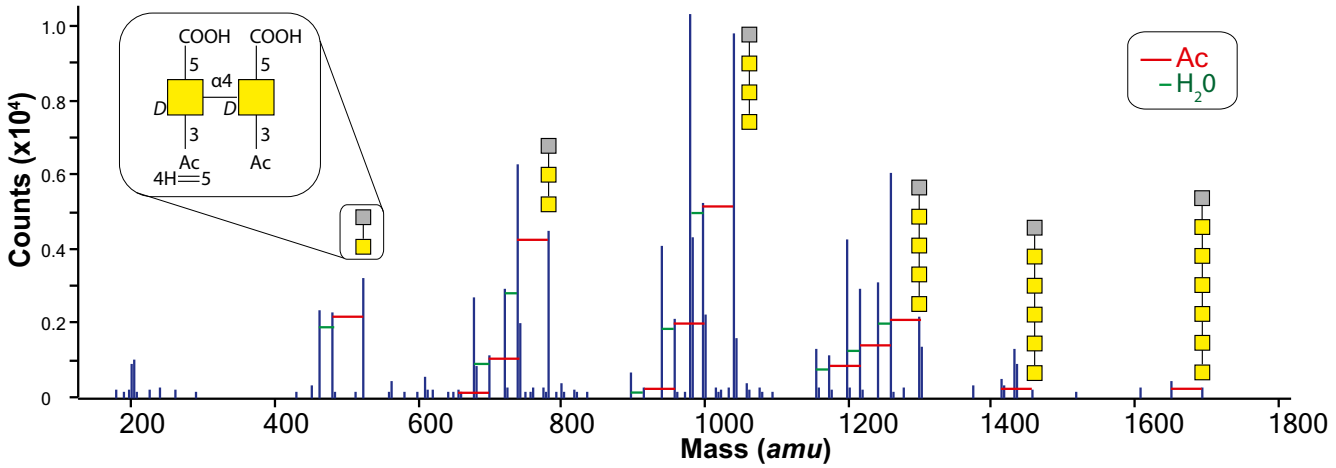

Fig. 3. Oligosaccharide profile of VexL reaction products. Shown is a charge-deconvoluted QToF mass spectrum of Vi antigen oligosaccharides generated by VexL depolymerization. Ions correspond to polymers of O-acetylated Hex*N*AcA residues, from two to seven residues in length (yellow box symbols), with a nonreducing terminal 4-deoxy-α-D-*galact*-4-enuronosyl residue (gray box). Species with nonstoichiometric O-acetylation [Δ42.010 atomic mass units (*amu*)] and/or water-loss (Δ18.010 *amu*) are indicated with red and green arrows, respectively.

while Arg^{172} and Asp^{171} hydrogen bond to Arg^{232} through water. VexL R172K had 44% of WT activity. Mutation of these "supporting" residues to alanine reduced lyase activity by ∼50% (*SI Appendix*, Fig. S3*F*), except for Arg^{172}, which was inactive (*SI Appendix*, Fig. S3 *E* and *F*).

The carboxylate of the central sugar is hydrogen bonded to both Gln^{231} and Tyr^{295}, and the oxygen atom of the *N*-acetyl group is hydrogen bonded to water (*SI Appendix*, Fig. S5*G*). The terminal oxygen atom of the *O*-acetyl group in this sugar is bridged to the protein by hydrogen bonds to a water molecule. The reducing sugar makes two hydrogen bonds to the protein, Arg^{305} with oxygen atom of the *N*-acetyl group and Tyr^{298} with the terminal oxygen atom of the *O*-acetyl group. In addition to the hydrogen bonds, all three sugars make extensive van der Waals contacts with the protein. Of particular note is the methyl group of the *O*-acetyl of the middle sugar, which sits in a hydrophobic pocket bounded by Tyr^{254} and Leu^{308}. Altering this pocket reduced depolymerase activity; VexL Y254F has 47% of WT activity (*SI Appendix*, Fig. S3*F*).

Table 1. Crystallographic data collection and refinement statistics

Data collection	
Space group	P 4_2 2_1 2
Cell dimensions	
a, *b*, *c*, Å	94.7, 94.67, 78.8
α, β, γ, °	90, 90, 90
Resolution, Å	60.6–1.22
(High resolution)	(1.24–1.22)
R_{merge}	0.07 (1.42)
$I/\sigma I$	17.0 (2.1)
Completeness, %	100 (100)
Average redundancy	12.8 (12.7)
Vm, $Å^3$/Da	2.05
Solvent, %	40.0
Refinement	
No. of unique reflections	106,029
R_{work}/R_{free}, %	14.0/16.6
No. of atoms (non-H)	
Protein	2,978
Water	243
Vi antigen	52
Malonate	7
B-factors, Å	
Protein	19.3
Water	29.7
Vi antigen	31.1
Malonate	35.4
rms deviations	
Bond lengths, Å	0.012
Bond angles, °	1.51
Ramachandran	
Favored, %	95.4
Disallowed, %	0
Molprobity score/centile	1.12/97
PDB	6FI2

Vi Antigen Envelope Translocation Includes a Periplasm-Accessible Intermediate. A predicted signal sequence suggested that VexL is an exported protein. Proteins reactive with VexL-specific antibodies were found associated with cells in three *Achromobacter* species (*SI Appendix*, Fig. S1*C*). However, no protein or lyase activity was detected in the spent media from cultures of these bacteria, indicating that VexL resides in the cytoplasm or periplasm of its natural host, rather than being a substrate for a protein secretion system (*SI Appendix*, Fig. S4*C*). Material reactive with Vi antigen-specific antibodies was identified in lysates of these *Achromobacter* species, suggesting that these *Achromobacter* do produce a glycan resembling Vi antigen (*SI Appendix*, Fig. S1*C*). To the best of our knowledge, CPS-specific depolymerases are not found in other ABC transporter-dependent assembly systems, and we reasoned VexL might offer insight into this process. However, investigating the role of VexL in Vi antigen production in *Burkholderiales* is complicated by the absence of information concerning both the diversity of polysaccharides it produces and the underlying biology (i.e., glycan function and growth conditions that affect Vi antigen synthesis). An additional barrier is the resistance of *Achromobacter* isolates to antibiotics used as markers in molecular genetic tools (26). We therefore chose to examine the impact of VexL in the characterized *S.* Typhi system. We argue that this heterologous system is a valid model to examine glycan accessibility in the export pathway because these organisms possess essentially identical Vi antigen biosynthesis and export proteins (*SI Appendix*, Fig. S1*A*). However,

MICROBIOLOGY

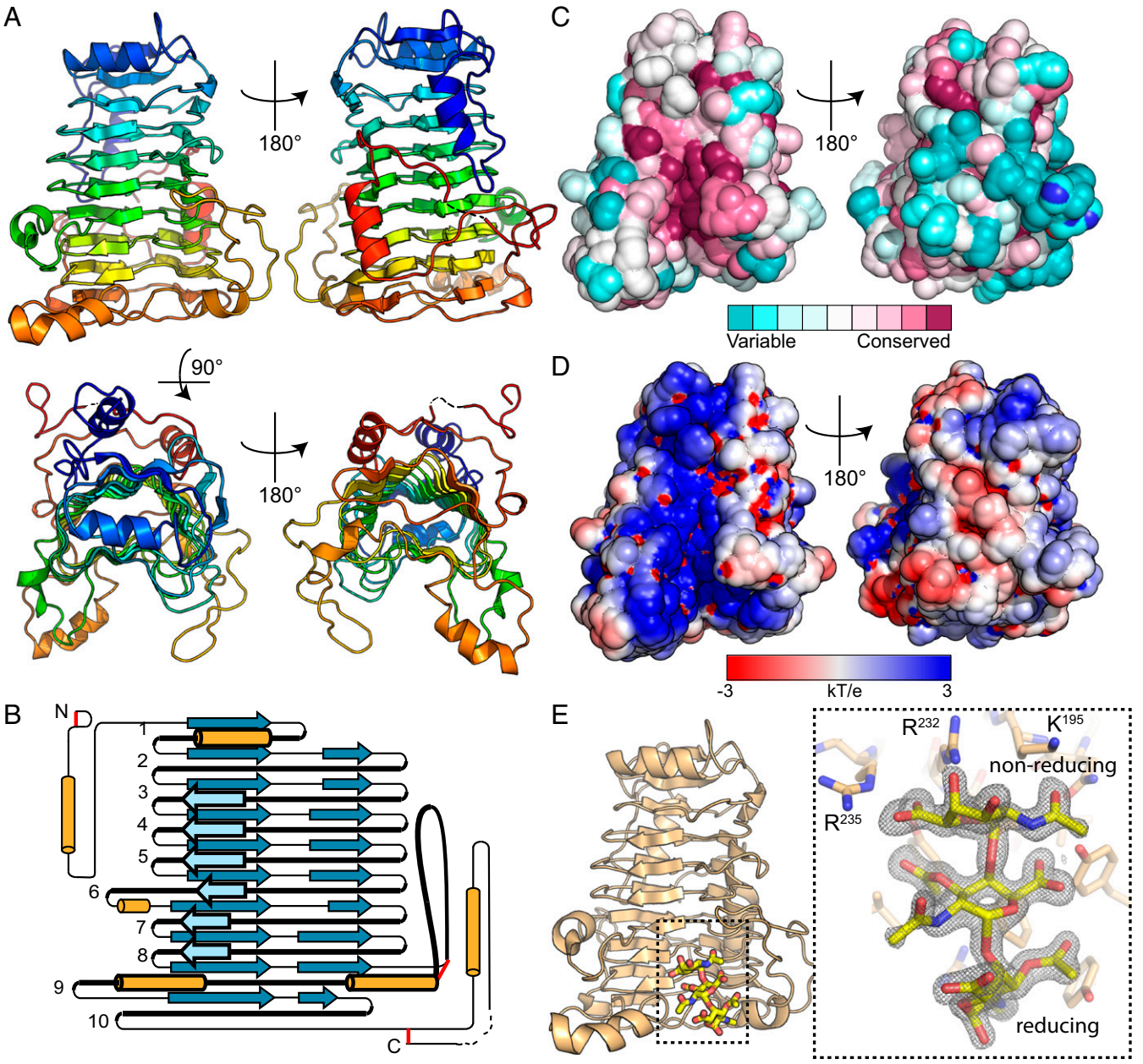

Fig. 4. Crystal Structure of *A. denitrificans* VexL-His$_6$ with bound Vi Antigen. (*A*) The graphic representation of VexL was generated from a 1.22-Å diffraction dataset collected from a single crystal of VexL-His$_6$ bound to a trisaccharide of purified Vi antigen. The diagram is colored in rainbow from N terminus (blue) to C terminus (red). (*B*) Topology of *A. denitrificans* VexL. Secondary structure elements are colored turquoise (β-sheets) or orange (α-helices). Disulfide linkages are colored red. Thick (3 pt) lines represent β-sheets and loops above the plane of the page. (*C*) Amino acid conservation of VexL with the bacterial and plant pectate lyases described in Fig. 2. Conservation scores were mapped to the VexL structure using ConSurf and displayed on the solvent-accessible surface (68). (*D*) Electrostatic surface potential for VexL was calculated at pH 6.5 using the Adaptive Poisson-Boltzmann Solver (66) and is displayed from −3 kT/*e* (red) to +3 kT/*e* (blue). (*E*) VexL structure with bound Vi antigen depicted as yellow sticks. (*Inset*) The $2F_O - F_C$ electron density map contoured at 1σ for the bound trisaccharide, as gray mesh. The reducing and nonreducing sugar residues are labeled.

S. Typhi does not encode VexL, and *A. denitrificans* does not encode TviA, a transcriptional activator of the Vi antigen locus unique to *S*. Typhi (27, 28).

S. Typhi was transformed with inducible plasmid vectors encoding *A. denitrificans* VexL-His$_6$, VexL R232A-His$_6$, or VexL$^{24\text{-}402}$-His$_6$ (which lacks the signal sequence). To confirm localization of these constructs in *S*. Typhi, released periplasmic contents were examined by immunoblotting employing VexL-specific antibodies. As expected, VexL and VexL R232A appeared in the periplasmic fraction whereas VexL$^{24\text{-}402}$ was confined to the cytoplasm and remained within spheroplasts (*SI Appendix*, Fig. S4*A*). Expression of VexL-His$_6$ reduced the average molecular weight of Vi antigen (Fig. 5*A*) while the catalytically inactive VexL R232A-His$_6$ (Fig. 5*A*) did not, confirming that the change in molecular weight is a specific catalytic effect rather than a structural consequence of overexpression of periplasmic VexL-His$_6$. In contrast, cytoplasmic VexL$^{24\text{-}402}$-His$_6$ had no effect on Vi antigen profiles (Fig. 5*A*), indicating that any degradation of product occurred postexport from the cytosol. The Vi antigen produced by cells expressing VexL variants was located on the cell surface in *S*. Typhi judged by susceptibility to the Vi antigen-specific bacteriophage ViII (Fig. 5*B*). Growth media from these cultures was examined, but

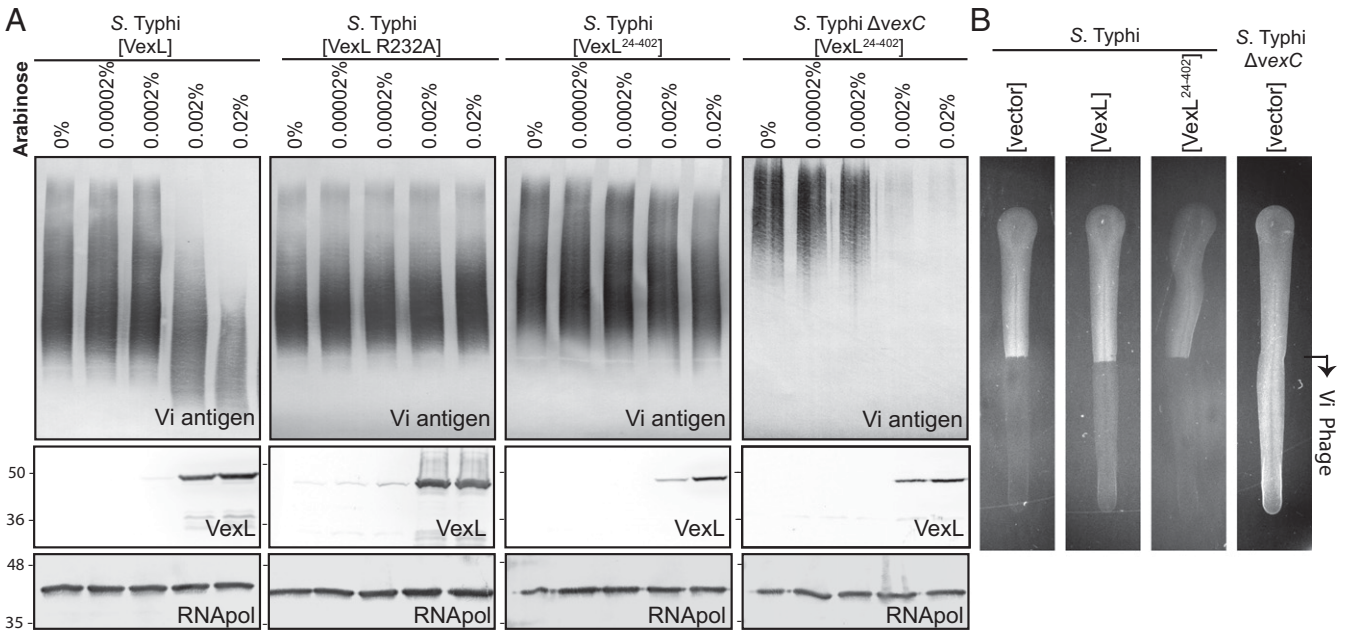

Fig. 5. Vi antigen is susceptible to degradation by VexL in the periplasm. (*A*) Expression of VexL in *S.* Typhi reduces the apparent molecular weight of Vi antigen in SDS/PAGE whereas VexL R232A and signal sequence-truncated VexL$^{24\text{-}402}$ do not. Deletion of the Vi antigen transporter NBD (*vexC*), renders (now cytoplasmic) Vi antigen susceptible to degradation by VexL$^{24\text{-}402}$. The figure depicts immunoblots of whole cell lysates, probed with Vi antigen-, VexL-, or RNA polymerase α-specific antibodies. RNA polymerase α was included as a loading control. Cultures were grown to midlog phase, before induction of plasmid-encoded protein expression with indicated final concentration of L-arabinose for 30 min. (*B*) Expression of VexL or VexL$^{24\text{-}402}$ does not eliminate susceptibility to lysis by a Vi antigen-specific bacteriophage (Vi phage II, HER no. 39). LB agar contained 0.02% (wt/vol) L-arabinose to induce plasmid-encoded gene expression. *S.* Typhi and *S.* Typhi Δ*vexC* provide positive and negative controls for surface-exposed Vi antigen, respectively.

no VexL protein was detected in the spent media by immunoblotting (*SI Appendix*, Fig. S4*B*). Moreover, no degradation of purified Vi antigen was evident after incubation with these media, unless the cells were mechanically disrupted (*SI Appendix*, Fig. S4*C*). These data ruled out any unanticipated effect occurring at the cell surface from small amounts of VexL released during growth. These experiments are entirely consistent with a model in which Vi antigen is protected within the cytoplasm during biosynthesis but exposed in the periplasm during translocation.

The inability of cytosolic VexL$^{24\text{-}402}$-His$_6$ to affect the Vi antigen profiles was surprising. To examine this phenotype in more detail, VexL$^{24\text{-}402}$-His$_6$ was expressed in *S.* Typhi Δ*vexC*, which lacks the ABC transporter NBD. This mutation interrupts Vi antigen export and leads to accumulation of glycan in the cytosol (14, 16). As expected, this strain was resistant to infection by bacteriophage ViII (Fig. 5*B*). In contrast to WT *S.* Typhi, *vexC* mutant Vi antigen was susceptible to degradation by VexL$^{24\text{-}402}$ (Fig. 5*A*), which confirmed that VexL$^{24\text{-}402}$ is active in vivo and can access its substrate if the normal assembly pathway is perturbed.

Discussion

VexL shares a conserved β-helical structure with diverse bacterial and plant catabolic polysaccharide lyases found in families PL1, PL3, and PL9 of the Carbohydrate-Active Enzyme (CAZy) database (29, 30). The representative structures of these protein families differ predominately in the position of loops inserted at turns that frame the glycan-binding site(s) but have little variation within the β-helix itself, suggesting that these elaborations are important for substrate recognition. Close structural homologs of VexL (*SI Appendix*, Fig. S5 and Table S4) belong to family PL1, which contains metal-dependent, endo-acting, pectin and pectate lyases with alkaline pH optima (24, 29). Despite the existence of dramatically different polysaccharide lyase folds [e.g., $(\alpha/\alpha)_3$ barrel, PL10], their catalytic centers for *trans*-β-elimination are conserved (31). The reaction employs an arginine residue positioned to extract a proton from C4 of the hexuronic acid residue in the +1 subsite (24). In VexL, we suggest that Arg^{232} fills this role. This is supported by inactivating mutations in VexL R232K (conservative) and R232A and the position of this residue relative to C4 of GalA$_4$ in the +1 subsite of the *Dickeya dadanti* PelC–GalA$_4$ complex (*SI Appendix*, Fig. S5*H*) (21). *D. dadanti* PelC includes an additional conserved arginine (Arg^{245}) (*SI Appendix*, Fig. S5*H*) that is involved in a ligand-positioning bidentate salt contact with the carboxylate of the GalA residue in the −1 subsite. In VexL, Arg^{235} fills this role (*SI Appendix*, Fig. S5*G*), and, as such, we propose that the trisaccharide of Vi antigen in the VexL structure represents glycan-binding subsites −3, −2, and −1. The hydrogen-bonding network involving Vi antigen *N*- and *O*-acetyl decorations (*SI Appendix*, Fig. S5*G*) is a critical component of substrate recognition; all point mutants of interacting residues had reduced lyase activity (*SI Appendix*, Fig. S3*F*). The specific requirement for the *O*-acetyl group is achieved not through a single interaction but rather through a network involving bridging water molecules. We propose that using a network, as opposed to a single interaction, underpins the tolerance of VexL for nonstoichiometric O-acetylation of its substrate. Notably, the VexL-binding groove lacks multiple DXD motifs, which coordinate divalent cations essential for glycan binding and activity in conventional pectate lyases, such as *D. dadanti* PelC (29) (*SI Appendix*, Fig. S5 *G* and *H*). The lack of sensitivity to EDTA supports the conclusion that VexL does not require a divalent cation(s) for catalysis. VexL has a signal peptide, a pH optimum more acidic than other relative enzymes (pH 5.5 vs. ∼8.0 to 9.5), and presence of multiple disulfide linkages that we suggest stabilize the N and C termini of the protein. Because of these unique properties, we propose that VexL has evolved unique structural changes and catalytic features that facilitate function in the more acidic (32) and oxidizing environment of the periplasm; VexL is a distinctive and unusual

addition to polysaccharide lyase family 1, that defines a robust subfamily with unusual polysaccharide lyase activity.

This work confirms that VexL is a periplasmic CPS-degrading enzyme. This feature is absent from all other known CPS assembly systems that use ABC transporters. However, periplasmic glycan-modifying proteins participate in production of some secreted exopolysaccharides (EPSs) that feature different biosynthesis and export machinery. These enzymes include polysaccharide lyases, hydrolases, epimerases, and acetylesterases that modify nascent EPS glycans nonstoichiometrically as they transit the periplasm. In some examples, these enzymes participate in the envelope translocation protein complex and are therefore sometimes required for glycan assembly and/or export. The *Pseudomonas aeruginosa* PEL polysaccharide provides an example. Unlike CPS, PEL does not possess a terminal lipid (33); its secretion requires a multidrug and toxic compound extrusion (MATE) transporter and a periplasmic scaffold that guides PEL to an outer membrane channel. PelA is a periplasmic PEL acetylesterase and hydrolase that binds the scaffold (34) and is required for PEL production (35). Similarly, *E. coli* poly-*N*-acetylglucosamine EPS employs a periplasmic acetylesterase (PgaB) that is required for export but not synthesis (36). In contrast, production of the (Wzx-dependent) *P. aeruginosa* PSL EPS does not require the cognate PslG periplasmic hydrolase although PslG overexpression decreases PSL production and biofilm formation (37). The *P. aeruginosa* EPS alginate assembly machinery encodes a periplasmic lyase (AlgL). AlgL is proposed to degrade periplasmic glycan that has escaped the export machinery, and deletion of *algL* does result in the accumulation of periplasmic glycan that results in cell lysis. However, AlgL also interacts with the secretion complex so interpretation of the phenotype is complicated (38, 39).

It is hard to argue that VexL would be required for Vi antigen export in the *Burkholderiales* given the overall similarity of the Vi antigen export machinery to examples from other bacteria, and homology to *S*. Typhi Vi antigen export proteins, which do not include VexL. The structure of VexL does not include any obvious domain that would point to an interaction with the CPS-translocation complex, and expressing a catalytically inactive VexL had no effect on the normal export process in *S*. Typhi. Furthermore, cognate periplasmic glycanases are not found in ABC transporter-dependent CPS assembly systems in other bacteria, which one would anticipate if this assembly strategy was intrinsically susceptible to aberrant and physiologically harmful accumulation of periplasmic glycan.

EPS/CPS produced by systems employing periplasmic glycan-depolymerizing or modifying enzymes do not share obvious structural features that might dictate a functional requirement for these enzymes. The EPS examples are frequently associated with biofilm formation, and this seems the most likely role for the Vi antigen-like glycan produced by the *Burkholderiales*. Although some *Achromobacter* isolates are opportunistic human pathogens (26, 40, 41), *vexL*-containing Vi antigen assembly loci are found predominantly in soil bacteria, where the role for Vi antigen has yet to be examined. Defining a biologically relevant role for any surface glycan is challenging without detailed information about the organisms' lifestyle and prevailing environmental conditions that might impact glycan production. Vi antigen is a major constituent of biofilm matrices in *S.* Typhi biofilms grown on gall stones ex vivo (42) but is apparently dispensable for biofilm formation in this setting (43). In contrast, Vi antigen production in *S.* Typhi is unequivocally linked to decreasing complement deposition and immune clearance (44). Vi production is up-regulated when *S.* Typhi enters intestinal epithelial cells, reduces complement and Toll-like receptor-dependent detection, and decreases recruitment of immune effectors to the site of infection (45–48). Vi antigen purified from *S.* Typhi is viscous; this property is related to glycan chain length and diminished by VexL treatment (16). It is therefore tempting to speculate that the gain or loss of an enzyme that alters the chain length, release, and/or quantity of CPS produced may be a critical factor in the function(s) of the Vi antigen in organisms with different physiologies and niches. How glycan depolymerizing and modifying activities contribute to biofilm formation is an open question. The relationships between quantity, chain length, physical properties, and function(s) of glycans in natural biofilms are currently poorly understood. However, the importance of EPS is reinforced by the successful application of EPS-specific glycanases as therapeutics to disrupt biofilms produced by pathogenic bacteria (4) and fungi (49, 50).

Regardless of its function in the natural host, VexL provided a molecular probe to generate important insight into the secretion machinery for Vi antigen in *S*. Typhi. Given the overall similarities in their export machineries, the findings are potentially relevant for other ABC transporter-dependent CPS assembly systems (2, 7). Understanding the details of these processes is vital in considering CPS as a therapeutic target in antivirulence strategies. We establish that the Vi antigen is protected from VexL degradation during its synthesis in the cytoplasm. This could be accomplished by a complex of biosynthetic enzymes creating a protected environment for the glycan or by tight coupling of polymerization and export, such that the glycan is exported as it is polymerized. Such coupling occurs in the synthesis of some O antigenic polysaccharides which couple a multiprotein synthesis complex to an ABC transporter (51, 52). Coupling synthesis and export of O antigen regulates product chain length, and a similar effect is evident in the increased molecular weight of Vi antigen in the *vexC* mutant (Fig. 5*A*). The observation that the Vi antigen becomes susceptible to cytoplasmic degradation in the absence of export suggests that there is normally a protected cytosolic "compartment" but does not on its own distinguish between an enveloping protein complex or coupling-mediated effect. However, the susceptibility of cytosolic Vi antigen accumulating in export-deficient mutants leads us to favor the latter explanation.

Previous studies used recombinant bacteriophage-derived endoglycanase enzymes to examine the cytoplasmic accessibility of CPS during its synthesis in *E. coli* K1 (53) and K5 (54). In both cases, CPS degradation was assessed by susceptibility of the bacteria to the corresponding CPS-specific bacteriophage (an indicator of some exported CPS). In K5, CPS production was directly quantified (54). Surprisingly, these studies yielded different conclusions. The authors concluded that K1 (53) was synthesized in a protected cellular compartment, but K5 was not (54). We recapitulated the experiments with *E. coli* K1 and found that it retained susceptibility to the CPS-specific bacteriophage (as reported in ref. 53), but, when the CPS was examined by immunoblotting, most was degraded by the cytoplasmic glycanase (*SI Appendix*, Fig. S6). This result is more consistent with those obtained with *E. coli* K5, and the different conclusions may reflect the different approaches and bacteriophages used to assess phenotypes. Neither system offers the cytoplasmic protection seen for Vi antigen, and this may reflect the differences in biosynthetic machinery and glycolipid acceptors used by *E. coli* and *S.* Typhi. The organization of the reported biosynthesis complex (53, 55, 56) would therefore appear to differ from that for Vi antigen.

Our results demonstrate that the Vi antigen can be degraded by VexL during the translocation phase in the periplasm. This finding is inconsistent with the current assembly model (Fig. 1) and raises questions that will only be answered with solved structures. The model was influenced by the ABC transporter-based tripartite drug efflux pumps (7), such as the MacA–MacB–TolC complex (11). A prototype OPX protein from the Wzx-dependent export of *E. coli* "Group 1" CPS forms a multimeric channel across the outer membrane (57) and interacts with its inner membrane (periplasm-exposed) PCP partner (58). In the

group 2 *E. coli* K5 system, a multiprotein complex has been detected that contains the ABC transporter (KpsMT), the PCP protein (KpsE), and the OPX protein (KpsD) (55). Furthermore, genetic data support cognate interaction between PCP-OPX protein pairs in other group 2 systems (59). Although there is currently no structural data for KpsD, the PCP protein KpsE forms a membrane-bound multimeric structure in cryo-EM whose periplasmic domain resembles the adaptor complex of tripartite drug efflux pumps (59). While the size and complexity of the CPS substrate and structures of efflux pumps have made the concept of a protected translocation pathway attractive as a working model, the accessibility of Vi antigen to degradation in the periplasm indicates that this must be reassessed. In group 1 systems, CPS polymerization occurs in the periplasm external to the PCP–OPX complex, and the glycan is proposed to access the lumen of the complex laterally (58). Site-directed cross-linking experiments established that CPS glycans transit the outer membrane within the OPX pore (60). The results presented here indicate that periplasmic access to the translocation pathway is also required in group 2 systems. Periplasmic exposure of the glycan may offer interesting avenues for CPS structural diversification. For example, LPS O antigens exported by ABC transporters are exposed during assembly/translocation and can be substrates for postpolymerization periplasmic glycosylation systems, creating altered structures and antigenic epitopes (61).

Experimental Procedures

Molecular Biology. Oligonucleotide primers were obtained from Sigma-Aldrich and are described in *SI Appendix*, Table S3. DNA fragments were generated by PCR employing primers that introduced restriction sites for use in cloning, digested using appropriate restriction enzymes (NEB; Invitrogen), and ligated to digested vector DNA using T4 DNA ligase (NEB). Site-directed mutants were generated using KOD HotStart DNA polymerase (Novagen) with primers containing point mutations (*SI Appendix*, Table S3), according to the QuikChange method (Stratagene). All DNA constructs were confirmed by sequencing at the Genomics Facility, Advanced Analysis Centre, University of Guelph, and are described in *SI Appendix*, Table S4.

Bioinformatic Analyses. Homologs of VexL were identified using a position-specific iterative BLAST search of the nonredundant protein sequence database. Initial hits from *Achromobacter* were selected to generate a VexL-specific blocks substitution matrix (BLOSUM), which was used in the second iteration (19). The top 500 hits were selected; hypothetical, predicted, "low-quality," and "multispecies" hits were removed. A multiple sequence alignment was generated using MUSCLE (62). *Dickeya dadanti* PelA, PelC, and *Bacillus sp.* N16-5 PelA were included in multiple sequence alignments due to structural similarity to VexL but did not appear as hits in position-specific iterative (PSI)-BLAST. Conserved blocks for phylogenetic analysis were defined using Gblocks (63). A maximum-likelihood phylogram was generated from 100 bootstrapped datasets using PhyML3.0 (64) and visualized by iTOL (65). Surface electrostatics were calculated using the Adaptive Poisson-Boltzmann Solver (APBS) (66). The PQR file, for use in APBS, was generated using PDB2PQR (67); pK_a were calculated by PROPKA at pH 6.5 (pH of crystallization). Conservation of amino acid residues was mapped to the VexL structure using ConSurf (68), employing the multiple sequence alignment and phylogram described above. Structural homologs of VexL were identified using PDBeFold (69). Figures were generated in PyMol (Schrödinger).

Purification of VexL-His$_6$ and Mutant Derivatives. For crystallography, *Achromobacter denitrificans* VexL was purified from the periplasm of *E. coli* C43 transformed with pWQ791, which encodes C-terminally hexahistidine-tagged VexL. Purification employed release of periplasmic contents by osmotic shock, followed by immobilized metal affinity and gel filtration chromatography, which was adapted from ref. 16 (*SI Appendix, Materials and Methods*).

Purification and VexL-Mediated Digestion of Vi Antigen. Vi antigen was purified from *S.* Typhi CWG1239 (Δ*vexE* Δ*waaG*::kan) using hot aqueous phenol extraction, hexadecyltrimethylammonium bromide precipitation, and enzymatic digestion of DNA/RNA/protein, and then by gel filtration chromatography (16). This polysaccharide lacks the terminal glycolipid residue that could have interfered with crystallization. Purified Vi antigen was incubated with purified VexL-His$_6$ and then analyzed by reversed-phase liquid chromatography (Agilent 1200, Extend-C18 column) coupled to tandem quadrupole time-of-flight (QToF) MS in negative ion mode (Agilent UHD 6530). See *SI Appendix, Materials and Methods* for details.

Lyase Enzyme Assay. VexL lyase activity was determined by spectrophotometric assay monitoring absorbance at 232 nm (*SI Appendix, Materials and Methods*) (25).

Crystallization of VexL-His$_6$, Crystallographic Data Collection, Refinement, and Analysis. Before crystallization, VexL-His$_6$ was diluted to 13.5 mg/mL (A_{280}) and incubated with purified Vi antigen at 5 mM (estimated based on the MW of $GalNAcA3Ac_4$, the most abundant product identified in MS; 1,036.27 g/mol) (Fig. 3). This mixture was incubated at 37 °C for 1 h and then centrifuged at 16,000 × *g*, 4 °C for 10 min before crystallization. Sparse matrix screening of the sample was performed using a combination of commercial and in-house crystallization screens. All experiments were set up as sitting drops, at 20 °C, using a Crystal Gryphon robot (Art Robbins) at drop ratios of 1:1 and 2:1 protein-precipitant in 300 and 450 nL of total drop sizes, respectively. After 1 d, UV-bright crystals were evident in 1.63 M sodium malonate, 0.1 M BisTris-HCl, pH 6.5, 0.08 M ammonium citrate, and 3.05% (vol/vol) 2-methyl-2,4-pentanediol. Drops were scaled up to 1.0 and 1.5 μL, and the mother liquor was refined to 1.58 M sodium malonate, 0.1 M BisTris-HCl, pH 6.5, 0.13 M ammonium citrate, and 2.5% (vol/vol) 2-methyl-2,4-pentanediol. To augment Vi antigen binding, 1 d before data collection, crystals were transferred to a drop of mother liquor supplemented with 10 mM Vi antigen and allowed to rest there overnight.

Crystals were harvested from Vi antigen-supplemented mother liquor and flash cooled directly in liquid nitrogen, without further addition of cryoprotectant. Data were collected at −173 °C on beamline id23-1 at the European Synchrotron Radiation Facility with automated data processing (70, 71). The structure was solved by molecular replacement using Balbes (72) via the online CCP4 server (73). Automatic model building was performed with Buccaneer (74), followed by manual rebuilding after interpretation in Coot (75). At this stage, density was visible to place a trisaccharide of Vi antigen. A library for Vi antigen was generated using PRODRG (76) and implemented during model refinement in REFMAC5 (77) and PDBREDO (78). The structure was validated using Molprobity (79) and deposited in the PDB (6FI2).

Subcellular Localization of VexL-His$_6$ and Mutant Derivatives. Cultures of *S.* Typhi H251.1 harboring plasmid-encoded VexL-His$_6$, or mutant derivatives, were grown in 250 mL of lysogeny broth using the conditions described in *In Vivo Lyase Accessibility Assay*. Periplasmic contents were released by osmotic shock (500 mM Sucrose, EDTA, and lysozyme) and further fractionated by differential centrifugation. These samples were then used for western immunoblotting. Spent cell-free culture media were concentrated and analyzed for the presence of VexL by immunoblotting and by incubating with purified Vi antigen. See *SI Appendix, Materials and Methods*.

In Vivo Lyase Accessibility Assay. Five milliliters of lysogeny broth cultures, supplemented with 100 μg/mL ampicillin, 0.2% (wt/vol) glucose, and 100 μg/mL 2,3-dihydroxybenzoic acid, were inoculated with *S.* Typhi H251.1, which harbored either pWQ791, pWQ935, or pWQ939, and grown for 16 h, at 37 °C. Then 1 OD_{600} unit equivalent of cells was collected and washed twice with 1 mL of sterile PBS and used to inoculate (at 1:1,000) 5 mL of fresh growth media without glucose. Cultures were grown at 37 °C until OD_{600} reached 0.5. Expression of the VexL derivatives was then induced with the indicated final concentrations of L-arabinose, and growth was continued for 30 min. One OD_{600} unit equivalent of cells was collected by centrifugation at 10,000 × *g* for 1 min, immediately resuspended in Laemmli loading buffer (80), and incubated at 100 °C for 10 min. Samples were then used for immunoblotting using Vi antigen-specific antibodies.

Bacteriophage-Sensitivity Assays. Half of an LB agar plate was inoculated with 3×10^8 pfu of bacteriophage Vi II (HER no. 39; Félix d'Hérelle Reference center for Bacterial Viruses, Université Laval) or 2×10^9 pfu of bacteriophage K1F (81). LB agar plates contained 100 μg/mL ampicillin and 0.02% (wt/vol) L-arabinose or 0.5 mM isopropyl β-D-1-thiogalactopyranoside (IPTG), to induce plasmid-encoded gene expression. Plates were dried at room temperature. Then, 8 μL of stationary-phase cultures were dropped onto the phage-free side of the plate and then tipped to the phage-inoculated area. Plates were incubated at 37 °C for 5 h and then imaged using an EPSON Perfection 2450 Photo scanner.

Generation of VexL-Specific Polyclonal Antibodies. Purified VexL-His_6 was resuspended at 50% (vol/vol) in Freund's incomplete adjuvant and used to immunize a female New Zealand white rabbit by intramuscular injection at four surgically prepared sites. The Animal Utilization Protocol was approved by the University of Guelph Animal Care Committee, and all procedures were performed by Animal Care Services at the Central Animal Facility at the University of Guelph. Antibodies were purified from sera by VexL-affinity chromatography, concentrated, and stored at −80 °C (*SI Appendix, Materials and Methods*).

PAGE and Immunoblotting. Whole-cell lysates were prepared by collecting 1 OD_{600} unit equivalent of cells resuspended in 100 μL of loading buffer (80). SDS/PAGE samples were incubated at 100 °C for 10 min, before electrophoresis [Tris-Glycine, 10% (wt/vol) acrylamide]. Protein gels were stained with Coomassie Brilliant Blue R-250. For immunoblotting, protein samples were transferred to nitrocellulose membranes (0.45 μm; Amersham Protran). Primary antibodies were murine monoclonal anti-His_5 (diluted 1:3,000; Qiagen), murine monoclonal anti-RNA polymerase α (sc-101597; diluted 1:2,000; Santa Cruz Biotechnology), murine anti-MalE (diluted 1:20,000; NEB), rabbit anti-OmpA (diluted 1:3,000; gift from Thomas Silhavy, Department of Molecular Biology, Princeton University, Princeton) (82), or purified polyclonal rabbit anti-VexL-His_6 (diluted 1:3,000; this work). Secondary antibodies were horseradish peroxidase (HRP)-conjugated goat anti-mouse (diluted 1:3,000; Qiagen) or HRP-conjugated goat anti-rabbit (diluted 1:3,000; Qiagen); detection employed HRP-substrate Luminata Classico (Millipore).

To analyze polysaccharides in whole-cell lysates, samples were prepared as above and then incubated with 50 μg of proteinase K for 1 h at 55 °C. The lysates were then separated by SDS/PAGE and transferred to PVDF or nylon membranes (BioDyne B; Pall). Membranes were probed with murine monoclonal anti-Vi antigen antibody P2B1G2/A9 (diluted 1:350) (83), or anti-polysialic acid-NCAM antibody (MAB5324 clone 2-2b, diluted 1:1,000; Millipore Sigma), followed by alkaline phosphatase-conjugated goat anti-mouse secondary antibody (diluted 1:3,000; Qiagen). Detection employed nitro-blue tetrazolium and 5-bromo-4-chloro-3-indolyl phosphate (Roche).

For purified polysaccharide, 1 μL of 2 M sucrose was added to 5 μL of sample (typically at 1 mg/mL Vi antigen) and loaded into 15% (wt/vol) acrylamide, 89 mM Tris, pH 7.6, 89 mM boric acid, and 2 mM EDTA minigels, for electrophoresis at 250 V for 70 min. Gels were stained for 16 h with 0.125% (wt/vol) Alcian blue, 10% (vol/vol) acetic acid, and 25% (vol/vol) ethanol, destained with 10% (vol/vol) acetic acid, 10% (vol/vol) ethanol for 1 h, and then developed using the Pierce Silver Stain kit.

ACKNOWLEDGMENTS. We gratefully acknowledge contributions of Jonah Nechacov in the early stages of this work. This work was supported in part by grants from the Canadian Institutes of Health Research (FDN_148364) (to C.W.). S.D.L. is a recipient of a Natural Science and Engineering Research Council Alexander Graham Bell Canada Graduate Scholarship and Michael Smith Foreign Study Supplement. C.W. is a Canada Research Chair. J.H.N. is a Wellcome Trust Investigator (100209/Z/12/Z).

1. Willis LM, et al. (2013) Conserved glycolipid termini in capsular polysaccharides synthesized by ATP-binding cassette transporter-dependent pathways in Gram-negative pathogens. *Proc Natl Acad Sci USA* 110:7868–7873.
2. Liston SD, Mann E, Whitfield C (2017) Glycolipid substrates for ABC transporters required for the assembly of bacterial cell-envelope and cell-surface glycoconjugates. *Biochim Biophys Acta* 1862:1394–1403.
3. Marshall JM, Gunn JS (2015) The O-antigen capsule of *Salmonella enterica* serovar Typhimurium facilitates serum resistance and surface expression of FliC. *Infect Immun* 83:3946–3959.
4. Taylor CM, Roberts IS (2005) Capsular polysaccharides and their role in virulence. *Contrib Microbiol* 12:55–66.
5. Whitfield C (2006) Biosynthesis and assembly of capsular polysaccharides in *Escherichia coli*. *Annu Rev Biochem* 75:39–68.
6. Islam ST, Lam JS (2013) Wzx flippase-mediated membrane translocation of sugar polymer precursors in bacteria. *Environ Microbiol* 15:1001–1015.
7. Willis LM, Whitfield C (2013) Structure, biosynthesis, and function of bacterial capsular polysaccharides synthesized by ABC transporter-dependent pathways. *Carbohydr Res* 378:35–44.
8. Locher KP (2016) Mechanistic diversity in ATP-binding cassette (ABC) transporters. *Nat Struct Mol Biol* 23:487–493.
9. Cuthbertson L, Mainprize IL, Naismith JH, Whitfield C (2009) Pivotal roles of the outer membrane polysaccharide export and polysaccharide copolymerase protein families in export of extracellular polysaccharides in gram-negative bacteria. *Microbiol Mol Biol Rev* 73:155–177.
10. Symmons MF, Bokma E, Koronakis E, Hughes C, Koronakis V (2009) The assembled structure of a complete tripartite bacterial multidrug efflux pump. *Proc Natl Acad Sci USA* 106:7173–7178.
11. Fitzpatrick AWP, et al. (2017) Structure of the MacAB-TolC ABC-type tripartite multidrug efflux pump. *Nat Microbiol* 2:17070.
12. Heyns K, Kiessling G (1967) Strukturaufklärung des vi-antigens aus *Citrobacter freundii* (*E. coli*) 5396/38. *Carbohydr Res* 3:340–353.
13. Kantele A, Pakkanen SH, Karttunen R, Kantele JM (2013) Head-to-head comparison of humoral immune responses to Vi capsular polysaccharide and Salmonella Typhi Ty21a typhoid vaccines–A randomized trial. *PLoS One* 8:e60583.
14. Wetter M, et al. (2012) Molecular characterization of the *viaB* locus encoding the biosynthetic machinery for Vi capsule formation in *Salmonella* Typhi. *PLoS One* 7: e45609.
15. Virlogeux I, Waxin H, Ecobichon C, Popoff MY (1995) Role of the viaB locus in synthesis, transport and expression of *Salmonella* typhi Vi antigen. *Microbiology* 141: 3039–3047.
16. Liston SD, Ovchinnikova OG, Whitfield C (2016) Unique lipid anchor attaches Vi antigen capsule to the surface of *Salmonella enterica* serovar Typhi. *Proc Natl Acad Sci USA* 113:6719–6724.
17. Marchler-Bauer A, et al. (2011) CDD: A Conserved Domain Database for the functional annotation of proteins. *Nucleic Acids Res* 39:D225–D229.
18. Petersen TN, Brunak S, von Heijne G, Nielsen H (2011) SignalP 4.0: Discriminating signal peptides from transmembrane regions. *Nat Methods* 8:785–786.
19. Altschul SF, et al. (1997) Gapped BLAST and PSI-BLAST: A new generation of protein database search programs. *Nucleic Acids Res* 25:3389–3402.
20. Thomas LM, Doan CN, Oliver RL, Yoder MD (2002) Structure of pectate lyase A: Comparison to other isoforms. *Acta Crystallogr D Biol Crystallogr* 58:1008–1015.
21. Scavetta RD, et al. (1999) Structure of a plant cell wall fragment complexed to pectate lyase C. *Plant Cell* 11:1081–1092.
22. Zheng Y, et al. (2012) Crystal structure and substrate-binding mode of a novel pectate lyase from alkaliphilic *Bacillus sp*. N16-5. *Biochem Biophys Res Commun* 420:269–274.
23. Seyedarabi A, et al. (2010) Structural insights into substrate specificity and the anti beta-elimination mechanism of pectate lyase. *Biochemistry* 49:539–546.
24. Yip VLY, Withers SG (2006) Breakdown of oligosaccharides by the process of elimination. *Curr Opin Chem Biol* 10:147–155.
25. Albersheim P (1966) [107] Pectin lyase from fungi. *Methods Enzymol* 8:628–631.
26. Bador J, Amoureux L, Blanc E, Neuwirth C (2013) Innate aminoglycoside resistance of *Achromobacter xylosoxidans* is due to AxyXY-OprZ, an RND-type multidrug efflux pump. *Antimicrob Agents Chemother* 57:603–605.
27. Winter SE, Raffatellu M, Wilson RP, Rüssmann H, Bäumler AJ (2008) The *Salmonella enterica* serotype Typhi regulator TviA reduces interleukin-8 production in intestinal epithelial cells by repressing flagellin secretion. *Cell Microbiol* 10:247–261.
28. Virlogeux I, Waxin H, Ecobichon C, Lee JO, Popoff MY (1996) Characterization of the *rcsA* and *rcsB* genes from *Salmonella* typhi: *rcsB* through *tviA* is involved in regulation of Vi antigen synthesis. *J Bacteriol* 178:1691–1698.
29. Hugouvieux-Cotte-Pattat N, Condemine G, Shevchik VE (2014) Bacterial pectate lyases, structural and functional diversity. *Environ Microbiol Rep* 6:427–440.
30. Cantarel BL, et al. (2009) The Carbohydrate-Active EnZymes database (CAZy): An expert resource for glycogenomics. *Nucleic Acids Res* 37:D233–D238.
31. Charnock SJ, Brown IE, Turkenburg JP, Black GW, Davies GJ (2002) Convergent evolution sheds light on the anti-beta -elimination mechanism common to family 1 and 10 polysaccharide lyases. *Proc Natl Acad Sci USA* 99:12067–12072.
32. Yang M, et al. (2014) Biocompatible click chemistry enabled compartment-specific pH measurement inside *E. coli*. *Nat Commun* 5:4981.
33. Franklin MJ, Nivens DE, Weadge JT, Howell PL (2011) Biosynthesis of the *Pseudomonas aeruginosa* extracellular polysaccharides, alginate, Pel, and Psl. *Front Microbiol* 2:167.
34. Marmont LS, et al. (2017) Oligomeric lipoprotein PelC guides Pel polysaccharide export across the outer membrane of *Pseudomonas aeruginosa*. *Proc Natl Acad Sci USA* 114:2892–2897.
35. Colvin KM, et al. (2013) PelA deacetylase activity is required for Pel polysaccharide synthesis in *Pseudomonas aeruginosa*. *J Bacteriol* 195:2329–2339.
36. Itoh Y, et al. (2008) Roles of *pgaABCD* genes in synthesis, modification, and export of the *Escherichia coli* biofilm adhesin poly-beta-1,6-N-acetyl-D-glucosamine. *J Bacteriol* 190:3670–3680.
37. Baker P, et al. (2015) Characterization of the *Pseudomonas aeruginosa* glycoside hydrolase PslG reveals that its levels are critical for Psl polysaccharide biosynthesis and biofilm formation. *J Biol Chem* 290:28374–28387.
38. Albrecht MT, Schiller NL (2005) Alginate lyase (AlgL) activity is required for alginate biosynthesis in Pseudomonas aeruginosa. *J Bacteriol* 187:3869–3872.
39. Jain S, Ohman DE (2005) Role of an alginate lyase for alginate transport in mucoid Pseudomonas aeruginosa. *Infect Immun* 73:6429–6436.
40. Gross R, et al. (2008) The missing link: *Bordetella petrii* is endowed with both the metabolic versatility of environmental bacteria and virulence traits of pathogenic *Bordetellae*. *BMC Genomics* 9:449.
41. Jakobsen TH, et al. (2013) Complete genome sequence of the cystic fibrosis pathogen *Achromobacter xylosoxidans* NH44784-1996 complies with important pathogenic phenotypes. *PLoS One* 8:e68484.
42. Marshall JM, Flechtner AD, La Perle KM, Gunn JS (2014) Visualization of extracellular matrix components within sectioned *Salmonella* biofilms on the surface of human gallstones. *PLoS One* 9:e89243.
43. Prouty AM, Schwesinger WH, Gunn JS (2002) Biofilm formation and interaction with the surfaces of gallstones by Salmonella spp. *Infect Immun* 70:2640–2649.

44. Keestra-Gounder AM, Tsolis RM, Bäumler AJ (2015) Now you see me, now you don't: The interaction of *Salmonella* with innate immune receptors. *Nat Rev Microbiol* 13: 206–216.
45. Tran QT, et al. (2010) The *Salmonella enterica* serotype Typhi Vi capsular antigen is expressed after the bacterium enters the ileal mucosa. *Infect Immun* 78:527–535.
46. Wangdi T, Winter SE, Bäumler AJ (2012) Typhoid fever: "You can't hit what you can't see". *Gut Microbes* 3:88–92.
47. Wilson RP, et al. (2011) The Vi capsular polysaccharide prevents complement receptor 3-mediated clearance of *Salmonella enterica* serotype Typhi. *Infect Immun* 79: 830–837.
48. Wilson RP, et al. (2008) The Vi-capsule prevents Toll-like receptor 4 recognition of *Salmonella*. *Cell Microbiol* 10:876–890.
49. Baker P, et al. (2016) Exopolysaccharide biosynthetic glycoside hydrolases can be utilized to disrupt and prevent Pseudomonas aeruginosa biofilms. *Sci Adv* 2: e1501632.
50. Snarr BD, et al. (2017) Microbial glycoside hydrolases as antibiofilm agents with cross-kingdom activity. *Proc Natl Acad Sci USA* 114:7124–7129.
51. Kos V, Whitfield C (2010) A membrane-located glycosyltransferase complex required for biosynthesis of the D-galactan I lipopolysaccharide O antigen in *Klebsiella pneumoniae*. *J Biol Chem* 285:19668–19687.
52. Kos V, Cuthbertson L, Whitfield C (2009) The *Klebsiella pneumoniae* O2a antigen defines a second mechanism for O antigen ATP-binding cassette transporters. *J Biol Chem* 284:2947–2956.
53. Steenbergen SM, Vimr ER (2008) Biosynthesis of the *Escherichia coli* K1 group 2 polysialic acid capsule occurs within a protected cytoplasmic compartment. *Mol Microbiol* 68:1252–1267.
54. Hudson T, Goldrick M, Roberts IS (2009) The *Escherichia coli* K5 capsule is not synthesized in a protected compartment within the cytoplasm. *J Bacteriol* 191: 1716–1718.
55. McNulty C, et al. (2006) The cell surface expression of group 2 capsular polysaccharides in *Escherichia coli*: The role of KpsD, RhsA and a multi-protein complex at the pole of the cell. *Mol Microbiol* 59:907–922.
56. Rigg GP, Barrett B, Roberts IS (1998) The localization of KpsC, S and T, and KfiA, C and D proteins involved in the biosynthesis of the *Escherichia coli* K5 capsular polysaccharide: Evidence for a membrane-bound complex. *Microbiology* 144:2905–2914.
57. Dong C, et al. (2006) Wza the translocon for *E. coli* capsular polysaccharides defines a new class of membrane protein. *Nature* 444:226–229.
58. Collins RF, et al. (2007) The 3D structure of a periplasm-spanning platform required for assembly of group 1 capsular polysaccharides in *Escherichia coli*. *Proc Natl Acad Sci USA* 104:2390–2395.
59. Larue K, Ford RC, Willis LM, Whitfield C (2011) Functional and structural characterization of polysaccharide co-polymerase proteins required for polymer export in ATP-binding cassette transporter-dependent capsule biosynthesis pathways. *J Biol Chem* 286:16658–16668.
60. Nickerson NN, et al. (2014) Trapped translocation intermediates establish the route for export of capsular polysaccharides across *Escherichia coli* outer membranes. *Proc Natl Acad Sci USA* 111:8203–8208.
61. Mann E, Whitfield C (2016) A widespread three-component mechanism for the periplasmic modification of bacterial glycoconjugates. *Can J Chem* 94:883–893.
62. Edgar RC (2004) MUSCLE: A multiple sequence alignment method with reduced time and space complexity. *BMC Bioinformatics* 5:113.
63. Castresana J (2000) Selection of conserved blocks from multiple alignments for their use in phylogenetic analysis. *Mol Biol Evol* 17:540–552.
64. Guindon S, et al. (2010) New algorithms and methods to estimate maximum-likelihood phylogenies: Assessing the performance of PhyML 3.0. *Syst Biol* 59: 307–321.
65. Letunic I, Bork P (2016) Interactive tree of life (iTOL) v3: An online tool for the display and annotation of phylogenetic and other trees. *Nucleic Acids Res* 44:W242–W245.
66. Jurrus E, et al. (2018) Improvements to the APBS biomolecular solvation software suite. *Protein Sci* 27:112–128.
67. Dolinsky TJ, et al. (2007) PDB2PQR: Expanding and upgrading automated preparation of biomolecular structures for molecular simulations. *Nucleic Acids Res* 35: W522–W525.
68. Landau M, et al. (2005) ConSurf 2005: The projection of evolutionary conservation scores of residues on protein structures. *Nucleic Acids Res* 33:W299–W302.
69. Krissinel E, Henrick K (2004) Secondary-structure matching (SSM), a new tool for fast protein structure alignment in three dimensions. *Acta Crystallogr D Biol Crystallogr* 60:2256–2268.
70. Nurizzo D, et al. (2006) The ID23-1 structural biology beamline at the ESRF. *J Synchrotron Radiat* 13:227–238.
71. Monaco S, et al. (2013) Automatic processing of macromolecular crystallography X-ray diffraction data at the ESRF. *J Appl Cryst* 46:804–810.
72. Long F, Vagin AA, Young P, Murshudov GN (2008) BALBES: A molecular-replacement pipeline. *Acta Crystallogr D Biol Crystallogr* 64:125–132.
73. Winn MD, et al. (2011) Overview of the CCP4 suite and current developments. *Acta Crystallogr D Biol Crystallogr* 67:235–242.
74. Cowtan K (2006) The Buccaneer software for automated model building. 1. Tracing protein chains. *Acta Crystallogr D Biol Crystallogr* 62:1002–1011.
75. Emsley P, Cowtan K (2004) Coot: Model-building tools for molecular graphics. *Acta Crystallogr D Biol Crystallogr* 60:2126–2132.
76. Schüttelkopf AW, van Aalten DMF (2004) PRODRG: A tool for high-throughput crystallography of protein-ligand complexes. *Acta Crystallogr D Biol Crystallogr* 60: 1355–1363.
77. Murshudov GN, Vagin AA, Dodson EJ (1997) Refinement of macromolecular structures by the maximum-likelihood method. *Acta Crystallogr D Biol Crystallogr* 53: 240–255.
78. Joosten RP, Long F, Murshudov GN, Perrakis A (2014) The PDB_REDO server for macromolecular structure model optimization. *IUCrJ* 1:213–220.
79. Chen VB, et al. (2010) MolProbity: All-atom structure validation for macromolecular crystallography. *Acta Crystallogr D Biol Crystallogr* 66:12–21.
80. Laemmli UK (1970) Cleavage of structural proteins during the assembly of the head of bacteriophage T4. *Nature* 227:680–685.
81. Vimr ER, Troy FA (1985) Identification of an inducible catabolic system for sialic acids (nan) in *Escherichia coli*. *J Bacteriol* 164:845–853.
82. Harms N, et al. (1999) Epitope tagging analysis of the outer membrane folding of the molecular usher FaeD involved in K88 fimbriae biosynthesis in *Escherichia coli*. *J Mol Microbiol Biotechnol* 1:319–325.
83. Qadri A, Ghosh S, Talwar GP (1990) Monoclonal antibodies against two discrete determinants on Vi capsular polysaccharide. *J Immunoassay* 11:235–250.
84. Benson DA, et al. (2017) GenBank. *Nucleic Acids Res* 45:D37–D42.